# Dielectric polymer composite with ultra-high thermal conductivity and low dielectric loss

*Xiangyan Yu[1], Muhammad Rehan Bhatti[1], Xintong Ren[1], Pietro Steiner[2,3], Federico Di Sacco[4,5], Ming Dong[6], Han Zhang[1], Dimitrios Papageorgiou[1], Giuseppe Portale[4,5], Coskun Kocabas[2,3], Cees WM Bastiaansen[1], Mike Reece[1], Haixue Yan[1], Emiliano Bilotti[1]**

[1]School of Engineering and Materials Science, Queen Mary University of London, London, UK.

[2]Department of Materials, University of Manchester, Manchester, UK.

[3]National Graphene Institute, University of Manchester, Manchester, UK.

[4]Physical chemistry of Polymeric and Nanostructured Materials, Zernike Institute for Advanced Materials, University of Groningen, Nijenborg 4, NL-9747 AG Groningen, The Netherlands.

[5]DPI, P.O. Box 902, 5600 AX Eindhoven, The Netherlands

[6]School of Physical and Chemical Sciences, Queen Mary University of London, London, UK.

*Corresponding Author email: e.bilotti@qmul.ac.uk

**ABSTRACT** Polymer based dielectric materials with simultaneously high thermal conductivity and low dielectric loss are highly desirable in various applications like energy storage, thermal management and electronic packaging. Polymer dielectrics generally benefit from good electrical insulation, high breakdown strength, high toughness and low density but suffer from very low thermal conductivity (0.1-0.5 $W \cdot m^{-1} \cdot K^{-1}$). Herein we propose a new strategy to overcome this compromise; solid-state drawing of ultra-high molecular weight polyethylene (UHMWPE) films doped with a small amount of nanodiamonds (NDs). The resulting orientation of UHMWPE macromolecules and the nanofiller significantly improves the thermal conductivity along the stretching direction, while the dodecane surface functionalization of the NDs endows a robust interface between the matrix and filler, which minimizes the thermal resistance and dielectric loss. Our film shows an ultra-high thermal

conductivity of 60 $W \cdot m^{-1} \cdot K^{-1}$ (with 2wt% NDs) in the drawing direction, very low dielectric loss, both at low and high electric field. More generally, herein we demonstrate that the interfaces introduced by the nanofillers do not necessarily cause an increase in dielectric loss at high electric field and a decrease in thermal conductivity, providing a new direction for the design of novel polymer based dielectric and functional materials.

---

**KEYWORDS:** thermal conductive polymer, low dielectric loss, capacitor, thermal management

## INTRODUCTION

The rapid development of high frequency, high power density and miniaturized electrical systems inevitably results in aggregated heat, which could lead to excessive temperatures, shorten the lifetime of electric equipment and even cause their malfunction. In order to prevent devices from heating up, expand their operating conditions and eliminate the necessity for cooling components, thermally conductive but electrically insulating materials are highly desired for applications in thermal management and capacitors, among others[1, 2].

However, polymers normally have very low thermal conductivity (typically less than 0.5 $W \cdot m^{-1} \cdot K^{-1}$)[3, 4]). There are two main strategies to improve their thermal conductivity: increase crystallinity and/or chain alignment and introduce fillers with high thermal conductivity[5, 6]. As for the first strategy, crystalline regions composed of stretched molecular chain should have very high thermal conductivity, considering that lattice vibrations can be transmitted 'unperturbed' along the chains[7].

Solid-state drawing has been used to increase the crystallinity and chain alignment of different polymers, notably polyethylene, thus increasing its thermal conductivity. Chen et al. used molecular dynamics simulations to calculate the thermal conductivity of a single polyethylene chain, which can be as high as 350 $W \cdot m^{-1} \cdot K^{-1}$ [8]. A thermal conductivity of 104 $W \cdot m^{-1} \cdot K^{-1}$ was reported for ultra-drawn UHMWPE nanofibers, which is higher than many metals but still lower than simulated maximum values due to the inevitable presence of defects (e.g. voids, entanglements, chain ends) in bulk material[9, 10]. For drawn UHMWPE films, only 60-65 $W \cdot m^{-1} \cdot K^{-1}$ was achieved with an ultra-high draw ratio of 200 because stretched films contain many more defects than short nanofibers. Besides, the thermal conductivity increased sharply at the beginning of drawing process, up to a draw ratio of about 60. Further drawing, up to a draw ratio of 200-240, causes even a decrease in thermal conductivity[7]. Micro-voids are produced by overdrawing, which not only scatter phonons and hinder the thermal transfer but also act as stress concentration point, therefore having a detrimental effect on mechanical strength and dielectric properties, counteracting the effect of chain alignment.[11]

The other common way to improve the thermal conductivity of polymer is the introduction of thermally conductive fillers. Examples of fillers are hexagonal boron nitride nanosheets (BNNs)[12-14]/nanotubes(BNNTs)[15], SiC[16], aluminum nitride (AlN)[17], aluminum oxide ($Al_2O_3$)[18], graphene[19] and nanodiamonds (NDs) [20, 21]. However, large amounts (usually higher than 10wt%) of (nano)fillers are required to form thermally conductive networks and produce a meaningful increase in thermal conductivity because of the large thermal resistance and phonon scattering at the polymer-filler and filler-filler interfaces[22]. For instance, Shengdu

et al. introduced nano-diamonds coated with silver nanoparticles and PDA (Ag-PDA-ND) into cellulose fiber (CNF) and measured an in-plane thermal conductivity of 16 $W \cdot m^{-1} \cdot K^{-1}$ with a filler loading of 15wt%.[23] A thermal conductivity of 19 $W \cdot m^{-1} \cdot K^{-1}$ was reported by adding hydroxyl-rich nano-diamonds (ND-OH) into poly(vinyl alcohol) (PVA) with a filler loading up to 90wt%.[24] Nevertheless, such high fractions of filler not only hampers the processability and deteriorates the final flexibility and ability to form high quality thin films, but also significantly increases the cost. Besides, the introduction of fillers often causes severe charge accumulation at the polymer/filler interface resulting a large mismatch of polarization and/or conductance between fillers and matrix and/or poor interface quality. As a consequence, the greatest majority of polymer nanocomposites reported in the literature show very high dielectric loss, compared with pristine polymers, especially under high electric field, hampering their use in electronic applications.[25] [26-31] Among other (nano)fillers, nanodiamonds possesses a unique combination of very high thermal conductivity (~2000 $W \cdot m^{-1} \cdot k^{-1}$) and high electrical insulation[32], making it a very promising filler to fabricate thermally conductive and electrically insulating films with low dielectric loss. Herein, we introduced nanodiamonds, surface functionalized with dodecane functional groups (NDs-dodecane), into a highly oriented ultra-high-molecular-weight-polyethylene (UHMWPE) polymer film, to obtain ultra-high thermal conductivity and low dielectric loss, both at low and high electric fields. The use of dodecane surface functionalization is of paramount importance in creating a robust interface, which minimizes both thermal resistance and dielectric loss. By tuning the filler content and solid-state drawing parameters, the resultant composite film with 2 wt% NDs and draw ratio of 60 shows an ultra-high thermal conductivity of 60 $W \cdot m^{-1} \cdot K^{-1}$ in the drawing direction with a low dielectric loss, both at low

electric field and at high electric field up to 400 $kV \cdot mm^{-1}$. This particular dielectric film shows great potential in applications like electronic packaging and capacitors as well as substrate technology, enabling microelectronic integrated circuits with accelerating speed and reducing size.[33]

## Experimental Section

### Materials

The ultra-high molecular weight polyethylene (UHMW-PE) was obtained from DSM Stamylan UH 034 (Royal DSM, the Netherlands) with a weight-average molecular mass of approximately $3.3 \times 10^6$ g/mol. This polymer grade has a melting temperature (Tm) of around 140 °C and average particle size (D50) of 150 μm. Xylene ($C_6H_4(CH_3)_2$, 98.5% mixture of isomers) was purchased from Thermo Fisher Scientific Inc. (the Netherlands). Dodecane functionalized nano-diamonds (NDs) with 65 nm diameter were purchased from Sigma Aldrich (901967). A small amount of NDs were burned at 450 ºC for 30mins using TGA 5500 to study the removal of the dodecane functionality. The obtained nano-diamonds was denoted as BNDs (bare nano diamond).

### Fabrication

UHMWPE (composite) films were prepared by solution casting and solid-state drawing (Figure 1e). NDs/UHMWPE composites specimens are defined as NDs-x-DR-y, pure UHMWPE specimen was defined as pure-DR-y, where *x* denotes the content of NDs and *y* the draw ratio. BNDs/UHMWPE composites specimens are defined in a similar way: BNDs-x-DR-y, where *x* denotes the content of BNDs and *y* the draw ratio. First, NDs (0.1, 0.3, 2 and 5wt% of UHMWPE) or BNDs (2wt% of UHMWPE) were dispersed in xylene under

ultrasonication at full power and room temperature for around 1 hour until visible aggregates disappeared. UHMWPE powder was then added to the dispersion before degassing with a second ultrasonication step at room temperature for 30 min. Subsequently, the mixture was stirred continuously in an oil bath at about 125 °C until the Weissenberg effect was observed. Then the mixture was kept at 125 ºC without stirring for 2 h to completely dissolve the UHMWPE in xylene (the UHMWPE solutions are all at 1 wt%). The solutions were then cast into aluminum trays and quenched to room temperature. Dry films were obtained after evaporating the xylene at room temperature for 7 days. Pure UHMWPE films were fabricated using the same procedure but without the dispersion and introduction of nanofillers. The optical images of obtained pure UHMWPE film, NDs2 and BNDs2 films before ultra-drawing were show in Figure 1f-h.The obtained films were subsequently cut into rectangular specimens (22 mm x 4.8 mm) and drawn in a two-stage drawing process to draw ratios (DR) $\lambda = 60$ at 120 °C (the first stage) and 125 ºC (the second stage), at a cross-head speed of 320 $mm \cdot min^{-1}$ using a universal tensile tester (Instron 5900R84, U.K.) equipped with an environmental chamber. The draw ratio of the drawn films was determined from the displacement of ink marks, which were marked on the surface of the strips at regular intervals of 2 mm before the drawing process. The optical image of sample NDs2-DR60 was show in Figure 1i.

Characterization

Scanning electron microscopy (SEM) (FEI Phenom, the Netherlands) analysis was carried out on the NDs and cross sections (cold-fractured in liquid nitrogen) of the nanocomposite films. Fourier transform infrared spectroscopy (FTIR) was performed on a Tensor 27

spectrometer (Bruker Optik GmbH, Ettlingen, Germany) with a platinum attenuated total reflectance (ATR) accessory. The scans were performed with a resolution of 4 $cm^{-1}$ in the wavenumber range of 4000-400 $cm^{-1}$. Raman spectroscopy was performed on a Renishaw inVia Raman Microscope using a 442 nm laser. The scans were performed with a 50s accumulation time and shift range of 3200-500$cm^{-1}$. Differential scanning calorimetry was performed on a differential scanning calorimetry (DSC) instrument (PerkinElmer DSC 4000) under nitrogen flow. The NDs/UHMWPE composites were heated and cooled at a rate of 10 $^{o}$C /min in a range from room temperature to 200 $^{o}$C . The crystallinity was calculated through enthalpy measurement of the melting peak area. Wide angle X-ray diffraction (WAXD) was carried out at the Multipurpose Instrument for Nano structural Analysis (MINA) at the University of Groningen, equipped with a Cu rotating anode emitting X-ray wavelength at 1.5413 Å (corresponding to 8 keV). The 2D scattering patterns were collected using a Bruker Vantec 500 2D, placed at 0.8 cm from the samples. The acquisition time was set to 2100 sec for each sample. Crystallographic orientation is quantified through calculation of the Herman's Orientation Factor[34]. Crystalline phase composition was calculated from the WAXD profiles using a home-made written MATLAB multi peaks deconvolution routine. WAXD reflections of the UHMWPE are fitted using a linear combination of Voigt functions. The amorphous halo was fitted using a Gaussian profile. The content of the crystalline phase is calculated by the ratio of the area of the Voigt peaks from the crystalline phase over the total profile area.[35, 36] UV-vis experiments were carried on a PerkinElmer LAMBDA 950 spectrophotometer at a 5 cm distance from the detector. All samples were coated with paraffin oil to avoid surface scattering, followed by sandwiching them between two glass slides (transparent at the tested wavelength range 300-700 nm) of about 1mm thickness each.

The thermal conductivity (K) was calculated using the following Equation:

$$K = C_H \rho \alpha \qquad (1)$$

Here, $C_H$ is the heat capacity (≈1.8 $J \cdot kg^{-1} \cdot K^{-1}$) of the samples, $\rho$ is the density (≈1000 kg $m^{-3}$) and $\alpha$ is the thermal diffusivity ($m^2 \cdot s^{-1}$). The thermal diffusivity ($\alpha$) was measured using a custom-built setup consisting of a pulsed (1 Hz) tunable laser beam (superK COMPACT supercontinuum), which excited heat waves that propagated periodically into the sample, and a high-resolution infrared camera (FLIR T660) as a detector. The camera was mounted with an IR micro-lens (pixel size 50 × 50). Thermal diffusivity was then calculated following the Angstrom method[37, 38]. For each sample (30 mm × 10 mm), 10 measurements were performed along the direction parallel to the solid-state drawing direction [39].

Gold electrodes with a thickness of around 100 nm and a diameter of 2 mm (for bipolar hysteresis loop measurements) or 5 mm (for dielectric spectroscopy measurements) were sputtered on both sides of drawn films. Bipolar hysteresis loops were obtained on a ferroelectric tester (NPL, Teddington, UK) at room temperature using a triangle waveform with a frequency of 10 Hz.[40] The tester can only generate a maximum voltage of 10 kV, which limits the field that can be applied to relatively thick specimens. The frequency dependence of dielectric properties was characterized using a Precision Impedance Analyzer (4294A, Agilent, Santa Clara, CA). A summary of the dielectric and thermal conductivity properties was presented in Table S1.

## RESULTS AND DISCUSSION

### 3.1 Structure characterization

Figure 1a-d shows the SEM images of surface functionalized NDs and the cross section of the composite films before ultra-drawing. Figure 1a reveals that the dodecane functionalized NDs have very uniform size, below 100 nm. Figure1b-d show the cross section of undrawn pure UHMWPE and UHMWPE/NDs composites films. The cross section of pure UHMWPE is relatively smooth, with a slight texture and no visible inclusions. In Figure 1c, the NDs appear as small white dots homogeneously distributed within the UHMWPE matrix. No visible aggregates are evident, demonstrating a good dispersion of the functionalized NDs when the nanoparticle content is less than 2 wt%. Some NDs agglomeration appears at higher filler content, shown by the presence of clusters of nearly one micrometer size for the NDs5 composites films (Figure 1d). The solid-state drawing process (Figure 1e) results in oriented films (8 – 13 micron) with good quality and even optical transparent (>93% at 550nm) for NDs concentrations lower than 2 wt% (Figure S6).

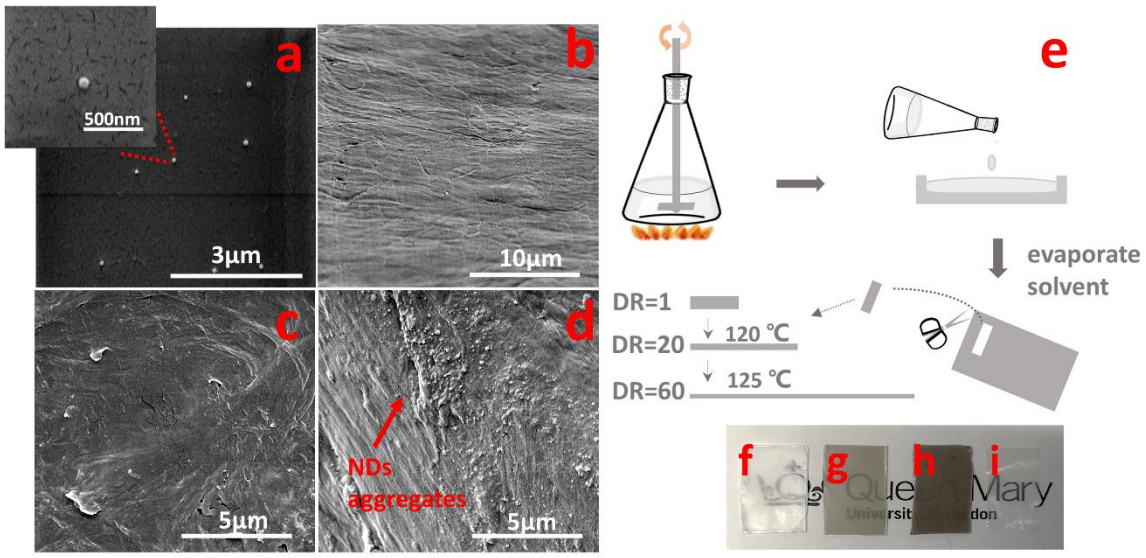

Figure 1. a-b) SEM images of: a) dodecane functionalized NDs; b) the cross section of undrawn pure UHMWPE sample; c) the cross section of undrawn NDs2 sample; d) the cross section of undrawn NDs5 sample; e) schematic illustration of fabrication method of the ultra-drawn NDs/UHMWPE composites. Optical images of: f) undrawn pure UHMWPE; g) undrawn NDs2 sample; h) undrawn BNDs2 sample and i) NDs2-DR60 sample.

Figure 2a shows the FTIR spectroscopy of the dodecane functionalized NDs. The broad peak at 3200-3400 $cm^{-1}$ is ascribed to the O-H stretching vibration from the -O-H functional group and absorbed water. The sharp peak at 2921-2848 $cm^{-1}$ originates from the C-H stretching vibration; the peaks at 1739 $cm^{-1}$, 1623 $cm^{-1}$ and 1460 $cm^{-1}$ originate from the ester carbonyl group, O-H in-plane deformation vibrations and C-H deformation vibrations, respectively; the 1260 and 1076 $cm^{-1}$ peaks is ascribed to the C-O stretching vibration. The sharp peak at 719 $cm^{-1}$ derives from the long chain deformation vibration of methene in the dodecane functional group. The nano-diamond core and the dodecane functional groups may be bonded by the ester group (ND-OOC-$C_{11}H_{23}$) at 1739 $cm^{-1}$, consistently with previously reported NDs modified with alkyl groups.[41] In the Raman spectroscopy of the filler, the peak at ~1330 $cm^{-1}$ derives from the diamond core (Figure 2b). [42]

The FTIR microscopy of drawn UHMWPE and UHMWPE/NDs nanocomposites (Figure 2d) shows four obvious peaks, all coming from the -$CH_2$ vibration. The peak and peak position of the NDs composites did not change with the loading of fillers. Characteristic peaks of -C=O and -O-H from the functionalized nano-diamonds are hardly detectable. Possible

reasons for this are the limited detection sensitivity (i.e. too low filler content) and limited penetration depth (polymer rich skin effect).

Figure 2e shows Raman spectroscopy of the drawn UHMWPE (pure-DR60) and the composite with 2wt% NDs loading (NDs2-DR60). The scattering bands of NDs2-DR60 and pure-DR60 differ mainly between 1500 to 1000 $cm^{-1}$. The 1400 to 1500 $cm^{-1}$ region includes three bands that are hard to separate from each other: 1414, 1438 and 1460 $cm^{-1}$. The 1414 $cm^{-1}$ peak comes from $CH_2$ bending in the crystalline phase; the 1438 $cm^{-1}$ and 1460 $cm^{-1}$ peaks come from the amorphous phase; the former is from a sort of random coil with several gauche bonds, the latter is from chains mainly of trans conformation but lacking regular packing. The higher intensity of the 1414 $cm^{-1}$ peak of NDs2-DR60 reveals higher crystallinity compared to pure-DR60. Peaks at 1129 and 1062 $cm^{-1}$ represent in-phase and out-of-phase all-trans C-C stretching vibrations, which comes from crystalline phase and extended chains in amorphous phase produced by the uniaxial-drawing. NDs2-DR60 shows much higher intensity of the band 1129 $cm^{-1}$ compared to pure-DR60, revealing a higher fraction of extended chains with all-trans C-C conformation which may come from the crystal phase and/or amorphous phase. Additionally, the relative strength of these two bands also differs; the addition of NDs gives rise to a higher intensity at 1129 $cm^{-1}$ than 1062 $cm^{-1}$. The possible reason is the reduced intensity of a broad scattering region centered at 1080 $cm^{-1}$, which is assigned to the C-C stretching of different kinds of gauche structures in unoriented amorphous phase composed of random coil. The broad band at 1080 $cm^{-1}$ is not detectable because it superposes with the 1062 $cm^{-1}$ peak, increasing the asymmetry and intensity of the latter. [43-46]

To further study the origin of the increased intensity of band 1129 $cm^{-1}$ by the introduction of NDs, we measured the crystallinity and crystal orientation of the drawn UHMWPE and the NDs/UHMWPE composites using WAXD and DSC (Figure 2). As for the crystal orientation, WAXD results shows that the introduction of NDs has a negligible influence on the Herman's Orientation Factor which means the NDs hardly change the orientation of drawn UHMWPE. As for the crystallinity, Both WAXD and DSC results show that the introduction of NDs also doesn't have a remarkable effect on the crystallinity. Therefore, we assume that the increased intensity of 1129 $cm^{-1}$ should come from the amorphous phase. The introduction of NDs increased the chain orientation of UHMWPE molecules in amorphous phase, possibly by facilitating the uniaxial-drawing process.

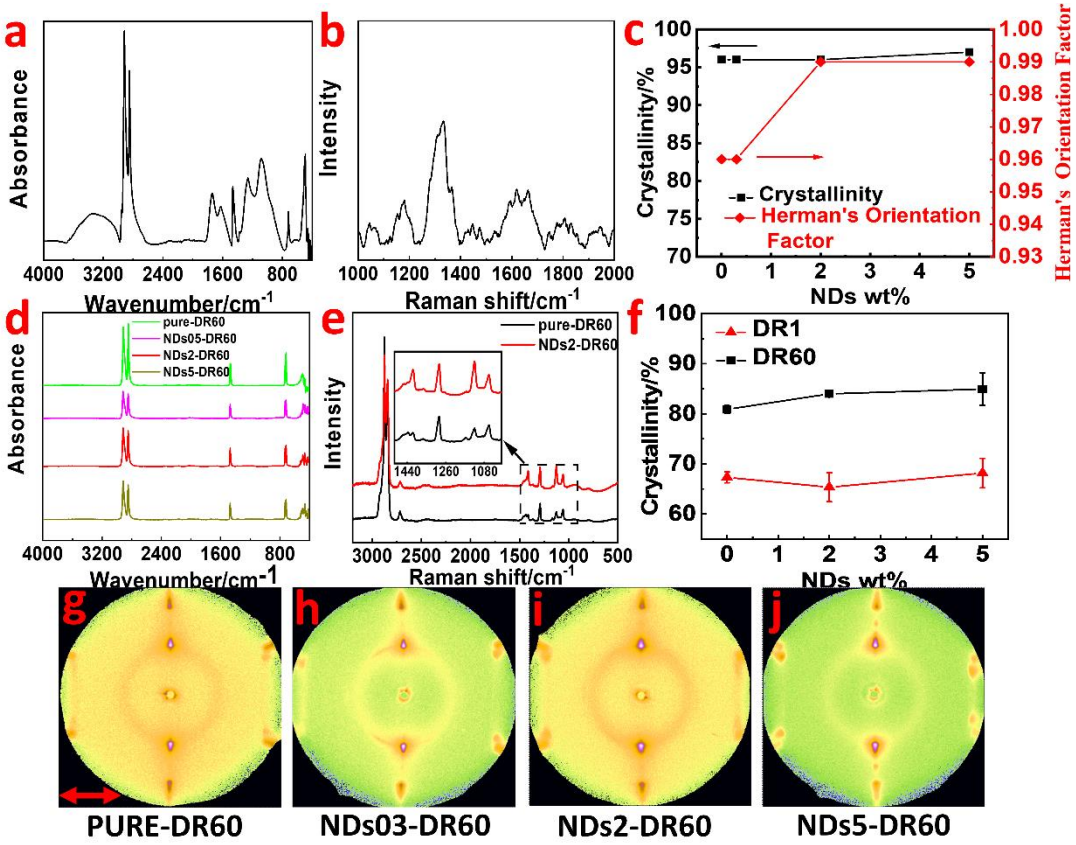

Figure 2. a) FTIR of dodecane functionalized NDs. b) Raman spectroscopy of NDs. c) Crystallinity and Herman's orientation factor obtained from the 2D WAXS patterns. d) FTIR of NDs/UHMWPE nanocomposites. e) Raman spectroscopy of pure-DR60 and NDs2-DR60 (the inset shows detailed spectroscopy in the region from 1600 to 800 $cm^{-1}$). f) Crystallinity of NDs/UHMWPE composites with draw ratio of 1 and 60, obtained from DSC measurement. g-j) 2D WAXS patterns of NDs/UHMWPE composites with draw ratio of 60. The red double arrow denotes the drawing direction.

3.2 Dielectric and thermal characterization

As for the dielectric properties (Figure 3), the relative dielectric permittivity remains similar after the introduction of NDs. For samples with draw ratio of 60, the dielectric loss (tanδ) is barely affected by filler loadings up to 5 wt%. The optimum loading content is 2 wt% with the tanδ slightly decreased from 0.007 for the matrix to 0.005 for NDs2 composite at 10 kHz. The difference of tanδ between the different samples is quite obvious in the lower frequency range ($10^3$ to $10^5$ Hz) but tends to diminish at $10^6$ Hz. This indicates that the difference in loss is related to relaxor dipoles with characteristic frequency below 1 MHz[47].

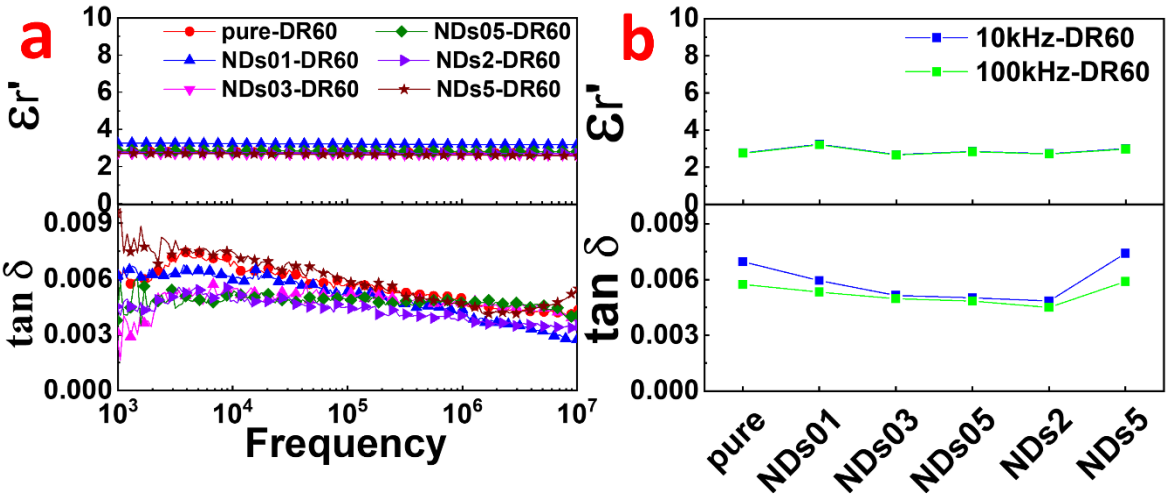

Figure 3. a) Dielectric constant and dielectric loss of NDs/UHMWPE composites with 60 draw ratio in the frequency range from $10^3$ to $10^7$. b) the dielectric constant and dielectric loss of NDs/UHMWPE composites with 60 draw ratio at 10 and 100 kHz.

Figure 4a-f shows the D-E loops and I-E loops of NDs/UHMWPE nanocomposites with draw ratio 60 with an applied electric field up to 400 kV·mm$^{-1}$. All the samples show slim D-E loops and rectangular I-E loops, which are indicative of their low loss at high field. Figure 4g summarizes the charge-discharge efficiency and dielectric loss at 400 kV·mm$^{-1}$. The charge-discharge efficiency ($\eta$) is defined as the ratio of the discharged electric energy to the charged electric energy calculated from the D-E loops. The obtained ND/UHMWPE composites exhibit an almost linear D-E behavior, like the pure UHMWPE. In the I-E loop measured at low frequency (10 Hz) triangular voltage waveform, the current has two main contributions: dielectric permittivity and electric conductivity. In our case, the former remains constant and corresponds to a constant current while the latter increases proportionally with electric field.[48] Therefore, the dielectric loss at high electric field, e.g. 400 kV·mm$^{-1}$ ($\tan\delta_{400}$), can be calculated by the equation below:

$$\tan\delta_{400}=\frac{I_2-I_1}{I_1} \qquad (2)$$

Where $I_1$ and $I_2$ were obtained from the I-E loop at 400 kV.mm$^{-1}$, representing the absolute value of the current (in *mA*) at zero electric field and 400 kV.mm$^{-1}$, respectively. The calculated results are plotted in Figure 4g. Consistent with the tanδ measured at low electric field, the charge-discharge efficiency and $\tan\delta_{400}$ first increased and then decreased with the NDs content. The NDs-05, with 0.5 wt% NDs, achieved the lowest $\tan\delta_{400}$ (~0.0416), while the $\eta$ barely changed up to a filler loading of 2 wt% (maximum amount of NDs that could be

dispersed well in UHMWPE). The decreased dielectric loss both at low field and high field may be related to the robust interface between the NDs and UHMWPE and the effect of the surface of the NDs trapping and demobilizing impurities and mobile charges.[49] However, when the filler content was increased to 5 wt%, aggregates appeared (Figure 1d) that acted as stress points, seriously decreasing the drawability of the UHMWPE matrix and causing more defects and even cracks.

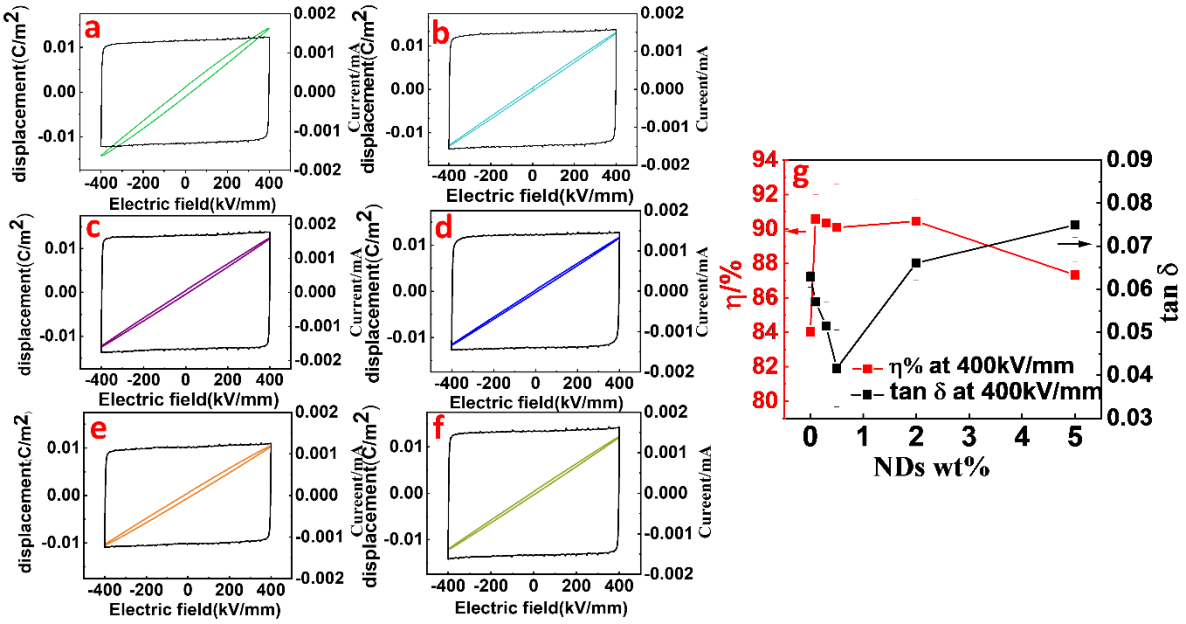


Figure 4.a)-f) the D-E loops and I-E loops of pure-DR60, NDs01-DR60, NDs03-DR60, NDs05-DR60, NDs2-DR60, NDs5-DR60 at 400kV/mm. g) The charge-discharge efficiency($\eta$) and dielectric loss ($\tan\delta_{400}$) of NDs/UHMWPE at 400kV/mm.

To verify the robust interface formed between the dodecane functionalities of NDs and UHMWPE and its benefits on dielectric properties, the NDs were heated at 450 ºC for 30 min in air to remove their organic coating before introducing them into UHMWPE films, followed by uniaxial drawing. XRD and FTIR characterization of the 'bare' NDs (BNDs) verified that the heating step removes all the dodecane groups without influencing the diamond core (Figure S1).

Specimen BNDs2-DR60 (UHMWPE with 2wt% BNDs and draw ratio 60) shows a tanδ of ~0.008 at 10 kHz, which is higher than pure-DR60 (tanδ~0.007) and NDs2-DR60 (tanδ~0.005) (Figure S2). Dielectric loss at 180 kV/mm ($\tan\delta_{180}$) were also calculated from I-E Loop. BNDs2-DR60 shows 5 times higher loss ($\tan\delta_{180}$~0.1229) than NDs2-DR60 ($\tan\delta_{180}$~0.0199) (Figure S3). After removing dodecane groups, the obtained BNDs are less compatible with UHMWPE, resulting in a poorer dispersion in the matrix (Figure S7) and a poorer interface, more vulnerable to external electric fields. Therefore, compared to NDs2-DR60 specimen, which can stand electric field higher than 400 kV/mm, the BNDs2-DR60 specimen failed at an electric field of 200 kV/mm. Besides, the dielectric loss at low and high electric field also increased significantly. This demonstrates the critical importance of a suitable NDs surface functionalization on the ultimate nanocomposite properties.

Figure 5a) shows the thermal conductivity of the drawn NDs/UHMWPE nanocomposites in the drawing direction. The very high thermal conductivity, compared with typical polymers, originates from the high orientation of molecular chain and nanofillers induced by solid-state drawing, and the formation of taut tie molecules, acting as inter-crystalline briges[50, 51]. The thermal conductivity in the drawing direction also increased with the NDs content, confirming the importance of the robust interface, which is consistent with the

dielectric results. The addition of 2 wt% NDs increased the thermal conductivity by 62% from 37 to 60 $W \cdot m^{-1} \cdot k^{-1}$. This value is much higher than, for instance, the reported NDs-PDMS composites with randomly dispersed NDs, showing a 15% increase in thermal conductivity with 2wt% of NDs.[52] We believe that the large increase of the thermal conductivity by NDs mainly comes from the non-crystalline region. Firstly, with the increasing crystallinity upon drawing (Figure 2c and f), the fraction of the NDs increases proportionally in the amorphous phase (the least thermally conductive phase) as NDs cannot be accommodated in the UHMWPE crystal lattice. Therefore, local thermally conductive pathways composed of highly aligned and thermally conductive NDs are formed between crystalline lamellas after uniaxial stretching (Figure S5). Secondly, Verified by Raman spectroscopy, DSC and 2-dimensional XRD (Figure 2), the chain orientation in non-crystalline region was also improved by the introduction of NDs. Last but not least, the interfacial thermal resistance in polymer nanocomposites usually results from differences between phonon spectra of different phases and scattering at the interfaces, largely hindering the thermal conductance. [1] While in our case, considering that dodecane has a similar chemical structure and thus refractive index with the matrix, the interfacial thermal resistance between the nanofillers and UHMWPE is minimized. [53, 54] As a result, The thermal conductivity of 60 $W \cdot m^{-1} \cdot k^{-1}$ of the NDs2-DR60 material is the highest value reported so far for any NDs-based polymer nanocomposite. [20, 21, 23, 24, 32, 52, 55-59] However, further increasing the filler content from 2 wt% to 5 wt% produced very limited further enhancement (from 60 to 61 $W \cdot m^{-1} \cdot k^{-1}$). This may be caused by NDs agglomerates (Figure 1c) which deteriorates the film quality and reduces the chain mobility during drawing, resulting in a large number of voids and thus increased phonon scattering.

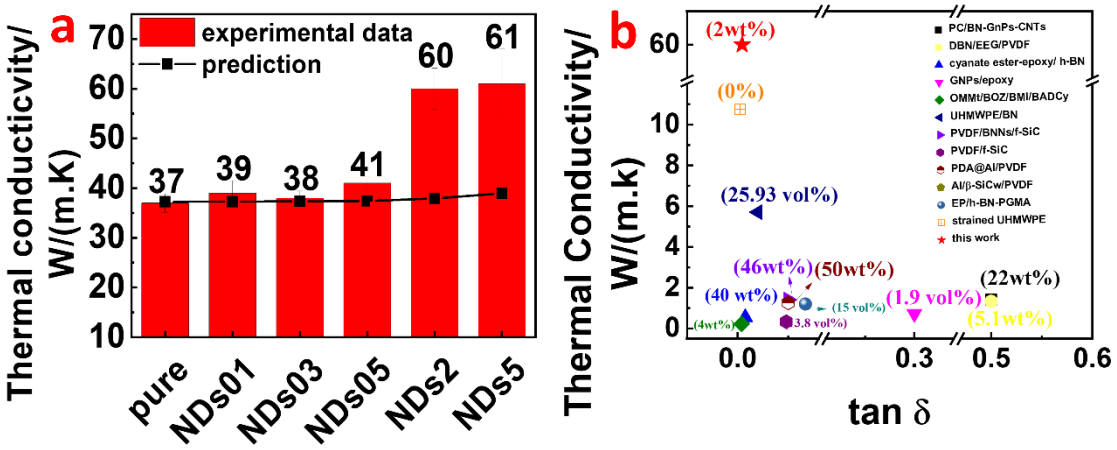


Figure 5. a) The thermal conductivity in the drawing direction of drawn nanocomposites with different NDs content and draw ratio of 60. Red bar represents measured thermal conductivity while the black line represents predicted thermal conductivity from Maxwell's equation. b) dielectric loss (tan δ) at 1000 Hz and thermal conductivity of the best performance composite film in this work (NDs2-DR60) and other work in previous literature. [60,61,62,63,64,65,28,30,66,67,68, 69]

Maxwell's equation (eq. 2) is an exact solution for the effect of randomly distributed and non-interacting spheres in a continuous medium.[21, 70] This equation can be used to predict the thermal conductivity of the NDs/UHMWPE composites and verify the contribution of NDs.

$$\lambda c=\lambda_m \frac{\lambda_f+2\lambda_m-2V_f(\lambda_m-\lambda_f)}{\lambda_f+2\lambda_m+V_f(\lambda_m-\lambda_f)} \quad (3)$$

$\lambda_m$, $\lambda_c$, $\lambda_f$ and $V_f$ represent the thermal conductivity of polymer matrix, composites, filler, and the volume fraction of the filler, respectively. In this work, $\lambda_m$ is 37 $W{\cdot}m^{-1}{\cdot}K^{-1}$ for UHMWPE with 60 draw ratio; the $\lambda_f$ is 2000 $W{\cdot}m^{-1}{\cdot}K^{-1}$.[71] The prediction of the thermal conductivity of NDs/UHMWPE nanocomposites with 60 draw ratio according to eq (2) is shown in Figure 5a. The measured thermal conductivities are much higher than the

predicted values: for NDs2-DR60, the thermal conductivity (~60 $W \cdot m^{-1} \cdot K^{-1}$ ) is 57% higher than predicted values. The discrepancy between the experimental data and predicted data using Maxwell's equation can be explained by the enhanced orientation and crystallinity upon uniaxial drawing. Figure 5b compares the results of thermal conductivity and dielectric loss at 1000 Hz in this work with the best results previously reported in the scientific literature. Our NDs2-DR60 film shows the best overall performance among polymeric dielectric thermal conductive composites with very high thermal conductivity but with low dielectric loss (see also Figure S4).

## 4 CONCLUSION

In summary, we have demonstrated that controlling the polymer/nanofiller interface and the orientation are effective strategies to overcome the typical detrimental effect of nanofillers on dielectric loss and high thermal resistance in polymer nanocomposites. Along with the positive effect of NDs on chain orientation of UHMWPE during uniaxial stretching, low dielectric loss (0.005) and very high thermal conductivity (60 $W.m^{-1}.k^{-1}$) is reported for NDs/UHMWPE nanocomposites films. These thermally conductive but electrically insulating films with very low loss could find application in thermal management, capacitor applications or as substrate material for high-speed signal transmission.

## DECLARATION OF COMPETING INTEREST

The authors declare that they have no known competing financial interests or personal relationships that could have appeared to influence the work reported in this paper.

## ACKNOWLEDGMENT

Xiangyan Yu (201906370046) was supported by a research studentship jointly funded by China Scholarship Council (CSC) and Queen Mary University of London.

## AUTHOR CONTRIBUTION

X.Y. produced samples and carried out most of the measurements. M.R.B. helped with producing samples. P.S. and C.K. contributed with the thermal conductivity measurement. F.D.S. and G.P. contributed with the 2D WAXD measurement. H.Y., M.J.R and X.R. participated in the analysis of dielectric properties. D.P., C.W.M.B and H.Z. helped with the analysis of thermal conductivity of this work. M.D. participated in the Raman measurement. E.B. initiated and mentored the work. All authors contributed to the preparation of the manuscript.

Appendix A. Supplementary data

## REFERENCES


1. Jiang, X. H. a. P., A Review of Dielectric Polymer Composites With High Thermal Conductivity

IEEE Electrical Insulation Magazine 2011, 0883-7554.

2. Moore, A. L.; Shi, L., Emerging challenges and materials for thermal management of electronics. *Materials Today* 2014, *17* (4), 163-174.

3. Dang, Z.-M., References. In Dielectric Polymer Materials for High-Density Energy Storage, Elsevier: pp 323-345.

4. Chaudhry, A. U.; Mabrouk, A.; Abdala, A., Thermally enhanced pristine polyolefins: fundamentals, progress and prospective. *Journal of Materials Research and Technology* 2020, *9* (5), 10796-10806.

5. Donovan, B. F.; Warzoha, R. J.; Cosby, T.; Giri, A.; Wilson, A. A.; Borgdorff, A. J.; Vu, N. T.; Patterson, E. A.; Gorzkowski, E. P., Strained Polymer Thermal Conductivity Enhancement Counteracted by Additional Off-Axis Strain. *Macromolecules* 2020, *53* (24), 11089-11097.

6. Saether, S.; Falck, M.; Zhang, Z. L.; Lervik, A.; He, J. Y., Thermal Transport in Polyethylene: The Effect of Force Fields and Crystallinity. *Macromolecules* 2021, *54* (13), 6563-6574.

7. Ronca, S.; Igarashi, T.; Forte, G.; Rastogi, S., Metallic-like thermal conductivity in a lightweight insulator: Solid-state processed Ultra High Molecular Weight Polyethylene tapes and films. *Polymer* 2017, *123*, 203-210.

8. Henry, A.; Chen, G., High Thermal Conductivity of Single Polyethylene Chains Using Molecular Dynamics Simulations. *Physical Review Letters* 2008, *101* (23), 235502.

9. Shen, S.; Henry, A.; Tong, J.; Zheng, R.; Chen, G., Polyethylene nanofibres with very high thermal conductivities. *Nat Nanotechnol* 2010, *5* (4), 251-5.

10. Carvill, J., 3 - Thermodynamics and heat transfer. In *Mechanical Engineer's Data Handbook*, Carvill, J., Ed. Butterworth-Heinemann: Oxford, 1993; pp 102-145.

11. Chae, H. G.; Kumar, S., Making Strong Fibers. *Science* 2008, *319* (5865), 908.

12. Chen, J.; Huang, X.; Sun, B.; Jiang, P., Highly Thermally Conductive Yet Electrically Insulating Polymer/Boron Nitride Nanosheets Nanocomposite Films for Improved Thermal Management Capability. *ACS Nano* 2019, *13* (1), 337-345.

13. Zeng, X.; Ye, L.; Yu, S.; Li, H.; Sun, R.; Xu, J.; Wong, C. P., Artificial nacre-like papers based on noncovalent functionalized boron nitride nanosheets with excellent mechanical and thermally conductive properties. *Nanoscale* 2015, *7* (15), 6774-81.

14. Zhu, H. L.; Li, Y. Y.; Fang, Z. Q.; Xu, J. J.; Cao, F. Y.; Wan, J. Y.; Preston, C.; Yang, B.; Hu, L. B., Highly Thermally Conductive Papers with Percolative Layered Boron Nitride Nanosheets. *ACS NANO* 2014, *8* (4), 3606-3613.

15. Zeng, X. L.; Sun, J. J.; Yao, Y. M.; Sun, R.; Xu, J. B.; Wong, C. P., A Combination of Boron Nitride Nanotubes and Cellulose Nanofibers for the Preparation of a Nanocomposite with High Thermal Conductivity. *ACS NANO* 2017, *11* (5), 5167-5178.

16. Gu, J.; Guo, Y.; Lv, Z.; Geng, W.; Zhang, Q., Highly thermally conductive POSS-g-SiCp/UHMWPE composites with excellent dielectric properties and thermal stabilities. *Composites Part A: Applied Science and Manufacturing* 2015, *78*, 95-101.

17. Xu, Y.; Chung, D. D. L.; Mroz, C., Thermally conducting aluminum nitride polymer-matrix composites. *Composites Part A: Applied Science and Manufacturing* 2001, *32* (12), 1749-1757.

18. Kozako, M.; Okazaki, Y.; Hikita, M.; Tanaka, T. In *Preparation and evaluation of epoxy composite insulating materials toward high thermal conductivity*, 2010 10th IEEE International Conference on Solid Dielectrics, 4-9 July 2010; 2010; pp 1-4.

19. Guo, F.; Shen, X.; Zhou, J.; Liu, D.; Zheng, Q.; Yang, J.; Jia, B.; Lau, A. K. T.; Kim, J. K., Highly Thermally Conductive Dielectric Nanocomposites with Synergistic Alignments of Graphene and Boron Nitride Nanosheets. *Advanced Functional Materials* 2020, *30* (19).

20. Song, N.; Cui, S.; Hou, X.; Ding, P.; Shi, L., Significant Enhancement of Thermal Conductivity in Nanofibrillated Cellulose Films with Low Mass Fraction of Nanodiamond. *ACS Applied Materials & Interfaces* 2017, *9* (46), 40766-40773.

21. Morimune, S.; Kotera, M.; Nishino, T.; Goto, K.; Hata, K., Poly(vinyl alcohol) Nanocomposites with Nanodiamond. *Macromolecules* 2011, *44* (11), 4415-4421.

22. Nan, C.-W.; Liu, G.; Lin, Y.; Li, M., Interface effect on thermal conductivity of carbon nanotube composites. *Applied Physics Letters* 2004, *85* (16), 3549-3551.

23. Yang, S.; Sun, X.; Shen, J.; Li, Y.; Xie, L.; Qin, S.; Xue, B.; Zheng, Q., Interface Engineering Based on Polydopamine-Assisted Metallization in Highly Thermal Conductive Cellulose/Nanodiamonds Composite Paper. *ACS Sustainable Chemistry & Engineering* 2020, *8* (48), 17639-17650.

24. Li, L.; Qin, Y.; Wang, H.; Li, M.; Song, G.; Wu, Y.; Wei, X.; Ali, Z.; Yi, J.; Song, S.; Lin, C.-T.; Jiang, N.; Yu, J., Improving thermal conductivity of poly(vinyl alcohol) composites by using functionalized nanodiamond. *Composites Communications* 2021, *23*, 100596.

25. Guo, F.; Shen, X.; Zhou, J.; Liu, D.; Zheng, Q.; Yang, J.; Jia, B.; Lau, A. K. T.; Kim, J.-K., Highly Thermally Conductive Dielectric Nanocomposites with Synergistic Alignments of Graphene and Boron Nitride Nanosheets. *Advanced Functional Materials* 2020, *30* (19), 1910826.

26. Gu, J.; Lv, Z.; Wu, Y.; Guo, Y.; Tian, L.; Qiu, H.; Li, W.; Zhang, Q., Dielectric thermally conductive boron nitride/polyimide composites with outstanding thermal

stabilities via in-situ polymerization-electrospinning-hot press method. *Composites Part A: Applied Science and Manufacturing* 2017, *94*, 209-216.

27. Gu, J.; Meng, X.; Tang, Y.; Li, Y.; Zhuang, Q.; Kong, J., Hexagonal boron nitride/polymethyl-vinyl siloxane rubber dielectric thermally conductive composites with ideal thermal stabilities. *Composites Part A: Applied Science and Manufacturing* 2017, *92*, 27-32.

28. Wang, B.; Yin, X.; Peng, D.; Zhang, Y.; Wu, W.; Gu, X.; Na, B.; Lv, R.; Liu, H., Highly thermally conductive PVDF-based ternary dielectric composites via engineering hybrid filler networks. *Composites Part B: Engineering* 2020, *191*, 107978.

29. Zhan, Y.; Ren, Y.; Wan, X.; Zhang, J.; Zhang, S., Dielectric thermally conductive and stable poly(arylene ether nitrile) composites filled with silver nanoparticles decorated hexagonal boron nitride. *Ceramics International* 2018, *44* (2), 2021-2029.

30. Wang, B.; Yin, X. H.; Peng, D.; Lv, R. H.; Na, B.; Liu, H. S.; Gu, X. B.; Wu, W.; Zhou, J. L.; Zhang, Y., Achieving thermally conductive low loss PVDF-based dielectric composites via surface functionalization and orientation of SiC nanowires. *Express Polymer Letters* 2020, *14* (1), 2-11.

31. Wang, T.; Wei, C.; Yan, L.; Liao, Y.; Wang, G.; Zhao, L.; Fu, M.; Ren, J., Thermally conductive, mechanically strong dielectric film made from aramid nanofiber and edge-hydroxylated boron nitride nanosheet for thermal management applications. *Composite Interfaces* 2020, 1-14.

32. Nan, B.; Wu, K.; Chen, W.; Liu, Y.; Zhang, Q.; Lu, M., Bioinspired modification strategy to improve thermal conductivity of flexible poly(vinyl alcohol)/nanodiamond

nanocomposite films for thermal management applications. *Applied Surface Science* 2020, *508*, 144797.

33. Song, Y.; Perez, C.; Esteves, G.; Lundh, J. S.; Saltonstall, C. B.; Beechem, T. E.; Yang, J. I.; Ferri, K.; Brown, J. E.; Tang, Z.; Maria, J.-P.; Snyder, D. W.; Olsson, R. H.; Griffin, B. A.; Trolier-McKinstry, S. E.; Foley, B. M.; Choi, S., Thermal Conductivity of Aluminum Scandium Nitride for 5G Mobile Applications and Beyond. *ACS Applied Materials & Interfaces* 2021, *13* (16), 19031-19041.

34. Wilchinsky, Z. W., Determination of orientation of the crystalline and amorphous phases in polyethylene by X-ray diffraction. *Journal of Polymer Science Part A-2: Polymer Physics* 1968, *6* (1), 281-288.

35. Ji, H.; Zhou, X.; Chen, X.; Zhao, H.; Wang, Y.; Zhu, H.; Ma, Y.; Xie, L., Deformation-Induced Crystallization Behavior of Isotactic Polypropylene Sheets Containing a β-Nucleating Agent under Solid-State Stretching. *Polymers* 2020, *12* (6), 1258.

36. Ryan, A. J.; Bras, W.; Mant, G. R.; Derbyshire, G. E., A direct method to determine the degree of crystallinity and lamellar thickness of polymers: application to polyethylene. *Polymer* 1994, *35* (21), 4537-4544.

37. Tomokiyo, A.; Okada, T., Determination of Thermal Diffusivity by the Temperature Wave Method. *Japanese Journal of Applied Physics* 1968, *7* (2), 128-134.

38. Cataldi, P.; Steiner, P.; Raine, T.; Lin, K.; Kocabas, C.; Young, R. J.; Bissett, M.; Kinloch, I. A.; Papageorgiou, D. G., Multifunctional Biocomposites Based on

Polyhydroxyalkanoate and Graphene/Carbon Nanofiber Hybrids for Electrical and Thermal Applications. *ACS Applied Polymer Materials* 2020, *2* (8), 3525-3534.

39. Wu, X.; Steiner, P.; Raine, T.; Pinter, G.; Kretinin, A.; Kocabas, C.; Bissett, M.; Cataldi, P., Hybrid Graphene/Carbon Nanofiber Wax Emulsion for Paper-Based Electronics and Thermal Management. *Advanced Electronic Materials* 2020, *6*.

40. Meng, N.; Ren, X.; Santagiuliana, G.; Ventura, L.; Zhang, H.; Wu, J.; Yan, H.; Reece, M. J.; Bilotti, E., Ultrahigh beta-phase content poly(vinylidene fluoride) with relaxor-like ferroelectricity for high energy density capacitors. *Nat Commun* 2019, *10* (1), 4535.

41. Krueger, A.; Boedeker, T., Deagglomeration and functionalisation of detonation nanodiamond with long alkyl chains. *Diamond and Related Materials* 2008, *17* (7), 1367-1370.

42. Mochalin, V.; Osswald, S.; Gogotsi, Y., Contribution of Functional Groups to the Raman Spectrum of Nanodiamond Powders. *Chemistry of Materials* 2009, *21* (2), 273-279.

43. Rull, F.; Prieto, A. C.; Casado, J. M.; Sobron, F.; Edwards, H. G. M., Estimation of crystallinity in polyethylene by Raman spectroscopy. *Journal of Raman Spectroscopy* 1993, *24* (8), 545-550.

44. Strobl, G. R.; Hagedorn, W., Raman spectroscopic method for determining the crystallinity of polyethylene. *Journal of Polymer Science: Polymer Physics Edition* 1978, *16* (7), 1181-1193.

45. Pigeon, M.; Prud'homme, R. E.; Pezolet, M., Characterization of molecular orientation in polyethylene by Raman spectroscopy. *Macromolecules* 1991, *24* (20), 5687-5694.

46. Boerio, F. J.; Koenig, J. L., Raman Scattering in Crystalline Polyethylene. *The Journal of Chemical Physics* 1970, *52* (7), 3425-3431.

47. Wilson, J. N.; Frost, J. M.; Wallace, S. K.; Walsh, A., Dielectric and ferroic properties of metal halide perovskites. *APL Materials* 2019, *7* (1), 010901.

48. YAN, H.; INAM, F.; VIOLA, G.; NING, H.; ZHANG, H.; JIANG, Q.; ZENG, T.; GAO, Z.; REECE, M. J., THE CONTRIBUTION OF ELECTRICAL CONDUCTIVITY, DIELECTRIC PERMITTIVITY AND DOMAIN SWITCHING IN FERROELECTRIC HYSTERESIS LOOPS. *Journal of Advanced Dielectrics* 2011, *01* (01), 107-118.

49. Shakun, A.; Anyszka, R.; Sarlin, E.; Blume, A.; Vuorinen, J., Influence of Surface Modified Nanodiamonds on Dielectric and Mechanical Properties of Silicone Composites. *Polymers* 2019, *11* (7), 1104.

50. Choy, C. L.; Chen, F. C.; Luk, W. H., Thermal conductivity of oriented crystalline polymers. *Journal of Polymer Science: Polymer Physics Edition* 1980, *18* (6), 1187-1207.

51. Peterlin, A., Plastic deformation of polyethylene by rolling and drawing. *Kolloid-Zeitschrift und Zeitschrift für Polymere* 1969, *233* (1), 857-862.

52. Ullah, M.; Kausar, A.; Siddiq, M.; Subhan, M.; Abid Zia, M., Reinforcing Effects of Modified Nanodiamonds on the Physical Properties of Polymer-Based

Nanocomposites: A Review. *Polymer-Plastics Technology and Engineering* 2015, *54* (8), 861-879.

53. Molefi, J. A.; Luyt, A. S.; Krupa, I., Comparison of the influence of copper micro- and nano-particles on the mechanical properties of polyethylene/copper composites. *Journal of Materials Science* 2010, *45* (1), 82-88.

54. AlMaadeed, M. A.; Nógellová, Z.; Mičušík, M.; Novák, I.; Krupa, I., Mechanical, sorption and adhesive properties of composites based on low density polyethylene filled with date palm wood powder. *Materials & Design* 2014, *53*, 29-37.

55. Song, N.; Cao, D.; Luo, X.; Guo, Y.; Gu, J.; Ding, P., Aligned cellulose/nanodiamond plastics with high thermal conductivity. *Journal of Materials Chemistry C* 2018, *6* (48), 13108-13113.

56. Cui, S.; Song, N.; Shi, L.; Ding, P., Enhanced Thermal Conductivity of Bioinspired Nanofibrillated Cellulose Hybrid Films Based on Graphene Sheets and Nanodiamonds. *ACS Sustainable Chemistry & Engineering* 2020, *8* (16), 6363-6370.

57. Sun, M.; Gao, G.; Dai, B.; Yang, L.; Liu, K.; Zhang, S.; Guo, S.; Han, J.; Zhu, J., Enhancement in thermal conductivity of polymer composites through construction of graphene/nanodiamond bi-network thermal transfer paths. *Materials Letters* 2020, *271*, 127772.

58. Zhang, Y.; Park, M.; Park, S.-J., Implication of thermally conductive nanodiamond-interspersed graphite nanoplatelet hybrids in thermoset composites with superior thermal management capability. *Scientific Reports* 2019, *9* (1), 2893.

59. Neitzel, I.; Mochalin, V.; Knoke, I.; Palmese, G. R.; Gogotsi, Y., Mechanical properties of epoxy composites with high contents of nanodiamond. *Composites Science and Technology* 2011, *71* (5), 710-716.

60. Jin, X.; Wang, J.; Dai, L.; Wang, W.; Wu, H., Largely enhanced thermal conductive, dielectric, mechanical and anti-dripping performance in polycarbonate/boron nitride composites with graphene nanoplatelet and carbon nanotube. *Composites Science and Technology* 2019, *184*, 107862.

61. Li, W.; Song, Z.; Qian, J.; Tan, Z.; Chu, H.; Wu, X.; Nie, W., Largely enhanced dielectric and thermal conductive properties of novel ternary composites with small amount of nanofillers. *Composites Science and Technology* 2018, *163*, 71-80.

62. Lei, Y.; Han, Z.; Ren, D.; Pan, H.; Xu, M.; Liu, X., Design of h-BN-Filled Cyanate/Epoxy Thermal Conductive Composite with Stable Dielectric Properties. *Macromolecular Research* 2018, *26* (7), 602-608.

63. Min, C.; Yu, D.; Cao, J.; Wang, G.; Feng, L., A graphite nanoplatelet/epoxy composite with high dielectric constant and high thermal conductivity. *Carbon* 2013, *55*, 116-125.

64. Wang, Y.; Wu, G.; Kou, K.; Pan, C.; Feng, A., Mechanical, thermal conductive and dielectrical properties of organic montmorillonite reinforced benzoxazine/cyanate ester copolymer for electronic packaging. *Journal of Materials Science: Materials in Electronics* 2016, *27* (8), 8279-8287.

65. Gao, C.; Lu, H.; Ni, H.; Chen, J., Structure, thermal conductive, dielectric and electrical insulating properties of UHMWPE/BN composites with a segregated structure. *Journal of Polymer Research* 2017, *25* (1).

66. Gong, Y.; Zhou, W.; Sui, X.; Kou, Y.; Xu, L.; Duan, Y.; Chen, F.; Li, Y.; Liu, X.; Cai, H.; Chen, Q.; Dang, Z.-M., Core-shell structured Al/PVDF nanocomposites with high dielectric permittivity but low loss and enhanced thermal conductivity. *Polymer Engineering & Science* 2019, *59* (1), 103-111.

67. Zhou, W.; Chen, Q.; Sui, X.; Dong, L.; Wang, Z., Enhanced thermal conductivity and dielectric properties of Al/β-SiCw/PVDF composites. *Composites Part A: Applied Science and Manufacturing* 2015, *71*, 184-191.

68. Jiang, Y.; Shi, X.; Feng, Y.; Li, S.; Zhou, X.; Xie, X., Enhanced thermal conductivity and ideal dielectric properties of epoxy composites containing polymer modified hexagonal boron nitride. *Composites Part A: Applied Science and Manufacturing* 2018, *107*, 657-664.

69. Li, Z.; An, L.; Khuje, S.; Tan, J.; Hu, Y.; Huang, Y.; Petit, D.; Faghihi, D.; Yu, J.; Ren, S., Solution-shearing of dielectric polymer with high thermal conductivity and electric insulation. *Science Advances* 2021, *7* (40), eabi7410.

70. Jiajun, W.; Xiao-Su, Y., Effects of interfacial thermal barrier resistance and particle shape and size on the thermal conductivity of AlN/PI composites. *Composites Science and Technology* 2004, *64* (10), 1623-1628.

71. Haggerty, S. E., A diamond trilogy: superplumes, supercontinents, and supernovae. *Science* 1999, *285* (5429), 851-60.